Lewis, S.R. and Read, P.L. (2003) "Equatorial jets in the dusty Martian atmosphere," *Journal of Geophysical Research* **108 (E4),** 5034, doi:10.1029/2002JE001933.

Equatorial Jets in the Dusty Martian Atmosphere

Stephen R. Lewis and Peter L. Read

Atmospheric, Oceanic and Planetary Physics, Department of Physics, Oxford University, Oxford, England

Abstract. We investigate the production of equatorial jets which demonstrate strong local super-rotation in an atmospheric general circulation model of Mars. These westerly jets are driven by diurnal thermal tides and their strength is shown to be closely related to the amount of dust in the atmosphere. The super-rotating jets are strongest near to equinox and under conditions of high atmospheric dust loading. If there is sufficient dust, in amounts corresponding to dust storm conditions, the westerly equatorial jets can occur at any time of year and reach speeds of over 40 m/s, peaking between 10 and 20 km altitude. For more moderate dust amounts, typical of background levels on Mars, the jets are still strong when the sub-solar point is close to the equator and latitudinally-symmetric, tidal modes are forced. Strong easterly, retrograde winds are also found high above the equator and it is shown that the thermal tides play a major role in their formation. This process is especially relevant close to equinox when the cross-equatorial meridional circulation is weak.

Introduction

The presence of dust in the Martian atmosphere is an important factor in the enhancement of direct local heating, primarily by the direct absorption of solar radiation in the case of moderate to high dust loadings [*Zurek et al.*, 1992]. Such an enhancement, of particular significance during major dust storms, can lead to substantial changes in the atmospheric circulation. In this study, we examine the effects of enhanced levels of dust in the Martian atmosphere on the angular momentum budget of the tropical atmosphere, as simulated in a general circulation model (GCM) of Mars [*Forget et al.*, 1999].

Global atmospheric super-rotation appears to be a ubiquitous feature of the atmospheres of slowly-rotating planets such as Venus and Titan, although it is far from clear that the same forcing processes are important in each case. Non-axisymmetric effects must be invoked in order to explain super-rotation [*Hide*, 1969]. In the case of Venus, those processes proposed include barotropic instabilities [*Gierasch*, 1975], solar-locked thermal tides [*Young and Schubert*, 1973; *Fels and Lindzen*, 1974; *Leovy*, 1987], and small-scale gravity waves [*Hou and Farrell*, 1987; *Gierasch*, 1987]. For a more complete review see, e.g. *Gierasch et al.* [1997].

Global super-rotation is less prominent on more rapidly-rotating planets such as the Earth and Mars. In the case of the Earth a small positive global super-rotation exists; *Read* [1986b] estimates super-rotation at $S = 0.015$, with S defined in Eqn. 5 below. Weak local super-rotation can also occur on Earth, particularly in the westerly phase of the Quasi-Biennial Oscillation (QBO) [*Andrews et al.*, 1987]. *Read* [1986a] argues that S is related to a global Rossby number, $V/\Omega a$, based on a typical flow speed V, rotation rate Ω and planetary radius a. Hence rapidly-rotating planets might typically be expected to exhibit less super-rotation than slow rotators, assuming roughly comparable wind speeds and radius, c.f. Earth and Venus.

We now focus on the production of significant local and global super-rotation on Mars, in the form of westerly, prograde, jets in the lower part of the atmosphere. Enhancements in the atmospheric dust loading, especially around the equinoxes, can lead to a strong amplification of the thermal tide and modes forced by the tide in association with the Martian topography [e.g., *Zurek et al.*, 1992; *Wilson and Hamilton*, 1996]. GCM simulations here show that the angular momentum transfers by these modes lead to the development of a significant prograde jet close to the equator in the lower atmosphere below about 40 km altitude.

Thermal tides are atmospheric gravity waves with peri-

ods which are harmonics of the solar day, forced by solar heating. Classical theory [*Chapman and Lindzen*, 1970] describes linearized disturbances about a stationary background state and has been applied to Venus and Mars, as well as to the Earth [e.g., *Lindzen*, 1970]. Tides are particularly prominent in the Martian atmosphere owing to the strong forcing per unit mass; for more detailed reviews of both theory and observations see, e.g. *Zurek et al.* [1992] and *Wilson and Hamilton* [1996]. The direct response to solar forcing is in sun-synchronous components, primarily westward-propagating zonal wavenumbers one and two. The wavenumber one, diurnal component propagates vertically in the tropics, with a vertical wavelength of around 30 km [*Wilson and Hamilton*, 1996], and tends to be vertically trapped at low levels in the extra-tropics. Vertical propagation, and the ability to transport and deposit momentum remotely, is an important feature when considering possible forcing mechanisms for super-rotation in the equatorial region. The wavenumber two, semi-diurnal tide has a much longer vertical wavelength, with little vertical phase propagation. Surface variations, primarily in topography, but also in thermal properties, can interact with the solar forcing to generate additional, non-sun synchronous tidal components. Most notably, in the case of Mars, the diurnal tide and zonal wavenumber two topographic variations can give rise to a westward-propagating wavenumber three and an eastward-propagating wavenumber one. The later diurnal, Kelvin mode has maximum amplitude at low latitudes and its frequency is close to atmospheric resonance, indicating the possibility of a large response [e.g., *Zurek*, 1976]. *Wilson* [2000] discusses the identification of a diurnal Kelvin mode in Mars Global Surveyor temperature data.

The observation that the atmosphere of Mars might exhibit local super-rotation under dusty conditions is not new. *Hamilton* [1982] and *Zurek* [1986] calculated Eliassen-Palm (EP) flux divergences and tidal zonal-mean forcing terms for Mars using classical tidal models and found that they could be large in the case of a dusty atmosphere. *Zurek and Haberle* [1988] applied such tendencies to a zonally symmetric model; their study did not produce local super-rotation, but concentrated only on a solsticial case. This is a time of year when the present results suggest that super-rotation is relatively small, although it is still significant at moderate to high dust loading. More recently, using a comprehensive GCM, *Wilson and Hamilton* [1996] noted the presence of local super-rotation in their simulations and attributed it to forcing by tidal modes, though they did not discuss the process in detail; these conclusions are supported by the model experiments described here. It is also possible to detect the presence of local super-rotation as weak westerly winds overlying the equator in other Martian GCMs [*Haberle et al.*, 1993; *Hourdin et al.*, 1995; *Forget et al.*, 1999], although, once again, most tend to concentrate on solsticial circulations when equatorial westerly flow is weak.

In this paper, we focus on the details of the production of equatorial prograde and retrograde jets, their evolution with time of year, possible implications for the global circulation of Mars and the prospects of obtaining observational evidence for their occurrence, perhaps during dust storms.

Model experiments

For this study, multi-annual integrations were conducted using the Oxford spectral version of the joint European Mars general circulation model (MGCM) [*Forget et al.*, 1999], run at T31 resolution (a truncation at total horizontal wavenumber 31) and with 25 levels in the vertical ranging between the surface and roughly 100 km altitude. Model results illustrated in this paper are cut-off at around 85 km altitude; three model layers at and above this point provide a "sponge layer" which applies Rayleigh friction to only the eddy components of the flow in order to limit wave reflections from the model top. The dust amount was prescribed to vary seasonally, modeled on the background level observed during the Viking Lander years without peaks for individual dust storm events [*Zurek and Martin*, 1993], and further described in *Lewis et al.* [1999].

The total dust optical depth for the baseline "Viking" scenario was specified to vary as a function of areocentric longitude, L_S (where $L_S = 0^\circ$ is northern spring equinox), peaking at $L_S = 280^\circ$,

$$\tau = 0.7 + 0.3\cos(L_S + 80^\circ), \tag{1}$$

where τ is the optical depth at a reference pressure $p_0 = 700\,\mathrm{Pa}$ and L_S is the areocentric longitude of Mars. The optical depth was taken to be uniform in the horizontal, but the top of the dust layer was specified as a function of both time and latitude,

$$z_{\max}(L_S, \phi) = \left(60 + 18\sin(L_S - 160^\circ) - 22\sin^2\phi\right)\ \mathrm{km}, \tag{2}$$

where ϕ is the latitude. The dust layer top $z_{\max}$ is a parameter in the equation which was used to describe the vertical variation of dust mixing ratio q,

$$q = q_0 \exp\left\{0.007\left[1 - (p_0/p)^{(70\ \mathrm{km}/z_{\max})}\right]\right\} \tag{3}$$

for pressure $p \le p_0$, with $q = q_0$ for $p > p_0$.

In order to study the effects of varying the degree of dust loading, the total dust optical depth in Eqn. 1 was also multiplied by two (τ =0.8–2.0, denoted "Viking×2" scenario) and by five (τ =2.0–5.0, denoted "Viking×5" scenario) for further multi-annual simulations. These experiments are not intended to represent realistic Martian years,

but the dust opacities lie well within the range of possible opacities observed on Mars during dust storms [*Zurek and Martin*, 1993], conditions which may persist for considerable periods of time (more than fifty days). Since the response of the atmosphere to increases in dust is relatively rapid, with a radiative timescale of one or two days [e.g., *Zurek et al.*, 1992], these scenarios should be representative of atmospheric states at a time when the dust loading is high.

Atmospheric super-rotation

The upper panel of Fig. 1 shows the zonal-mean zonal wind on a constant pressure surface at 136 Pa, equivalent to about 15 km altitude above the surface, as a function of latitude and areocentric longitude for a full Martian seasonal cycle of the prescribed Viking dust scenario. The pattern of zonal-mean winds is essentially repeatable from year to year (it is the second year of simulation that is shown here). Strong westerlies (prograde zonal winds) can be seen in each winter hemisphere with mostly weaker easterlies in the summer hemispheres. Of most immediate interest to this paper is the observation that, centered around the time of the equinoxes ($L_S = 0^\circ$ and $L_S = 180^\circ$), the flow can be westerly over the equator. This immediately indicates that the atmosphere in the equatorial region is rotating more rapidly than would be possible by redistribution of angular momentum from an initially solid-body rotation state, and thus shows the presence of local super-rotation.

The axial angular momentum per unit mass of the atmosphere, m, is given by

$$m = \Omega a^2 \cos^2 \phi + ua \cos \phi, \tag{4}$$

where Ω is the planetary rotation rate, a the planetary radius (3396 km), u the zonal wind and ϕ the latitude. Global super-rotation, S, can be defined as the mass-weighted integral of m over the whole volume of the atmosphere, compared to the same integral for an atmosphere at rest, denoted M_0,

$$S = \left(\iiint m \, a^2 \cos \phi d\lambda d\phi dp/g \right) /M_0 - 1, \tag{5}$$

where λ is longitude, p is pressure and g is gravitational acceleration. It is then possible to define a local super-rotation index, based on the specific angular momentum derived from the zonal-mean zonal wind, $\overline{u}$,

$$s = \overline{m}/\Omega a^2 - 1, \tag{6}$$

with $s > 0$ indicating local super-rotation.

The lower panel of Fig. 1 contours positive values of s on the 136 Pa pressure surface and indicates that super-rotation indeed occurs for large parts of the Martian year within 20° of the equator, peaking at the equinoxes with $s = 0.073$. This surface is close to the peak of the westerly equatorial jet; in fact, the maximum local super-rotation seen on any level is $s = 0.077$. The global super-rotation measured at this season is $S = 0.045$, about three times higher than that calculated for Earth [*Read*, 1986a]. The variability in dust loading with time of year in the Viking scenario (Eqn. 1), in combination with the variation in solar heating resulting from the ellipticity of the Martian orbit, accounts for much of the asymmetry in the zonal wind with time of year seen in Fig. 1. A similar plot for the Viking$\times$5 scenario is shown in Fig. 2. This confirms that increasing the amount of dust in the atmosphere increases the degree of super-rotation with s now positive at almost all times of year and up to 30° from the equator, peaking at $s = 0.161$, with global super-rotation increasing less dramatically to $S = 0.058$. Results for the Viking$\times$2 scenario (not shown) are intermediate, with peak values of $s = 0.109$ and $S = 0.050$.

The equatorial westerly jet at northern autumn equinox can be seen clearly in Fig. 3 in the lower atmosphere between the surface and 40 km altitude, peaking close to 15 km at westerly wind speeds of more than 40 m/s in the dustiest conditions. Figure 3 also shows the distribution of local super-rotation with latitude and height, indicating that a substantial fraction of the atmosphere is locally super-rotating at this time of year.

Figure 4 shows the equivalent zonal-mean cross-sections of zonal wind and super-rotation in northern summer, a time when the atmosphere is super-rotating much less spectacularly, though prograde flow above the equator is still clearly evident. At this time the jets visible in Fig. 3 are beginning to grow. Further diagnostics for this period of equatorial jet growth are discussed in Section .

Figures 5 and 6 show the mean meridional flow streamfunction, averaged over the same periods shown in Figs. 3 and 4. These diagrams are restricted to within 45° of the equator, and to below about 40 km in altitude, in order to focus on the region of equatorial super-rotation. For the period immediately following equinox, Fig. 5, the mean circulation tends to be relatively weak and to form a pattern of cells with rising motion above the equator itself. Most strikingly, under high dust conditions when the region of maximum solar heating is higher in the atmosphere, the cells appear to form a quadrupole pattern with horizontal convergence and vertical divergence at around 10 km altitude over the equator. The pattern of four cells in the meridional circulation appears to be induced by the presence of atmospheric tidal components, forced most strongly, symmetrically about the equator at equinox. In experiments without tidal forcing, shown in the following section, the meridional circulation

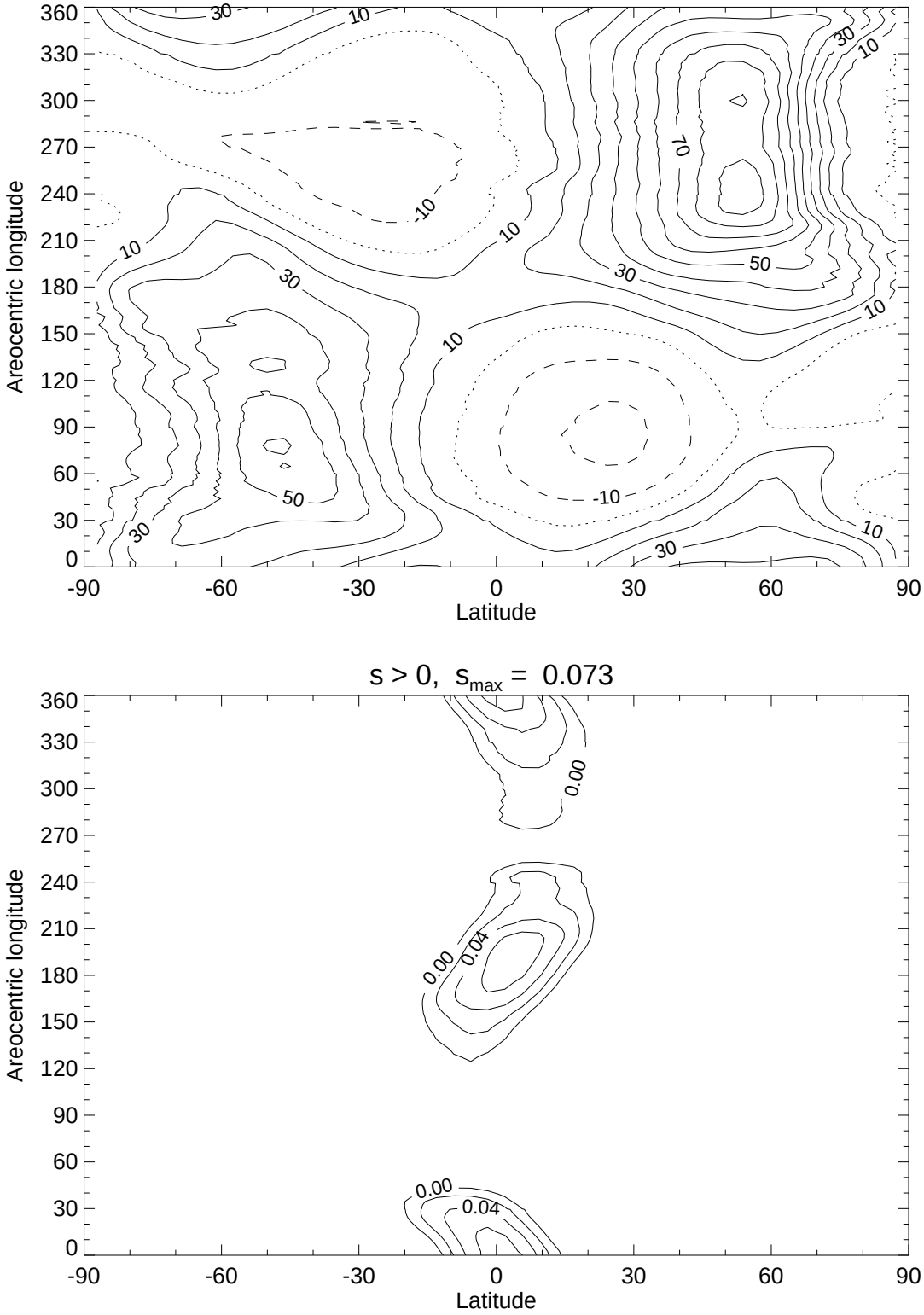

Figure 1. Zonal-mean zonal wind, $\overline{u}$ (upper panel), and local super-rotation index, s (lower panel), on the 136 Pa pressure surface under the Viking dust scenario. The wind has been smoothed in time to remove any variations with periods of less than 5 days for clarity. In this, and future plots, positive contours are shown as solid, the zero contour is dotted and negative contours are dashed. Only positive values of s are contoured, with an interval of 0.02.

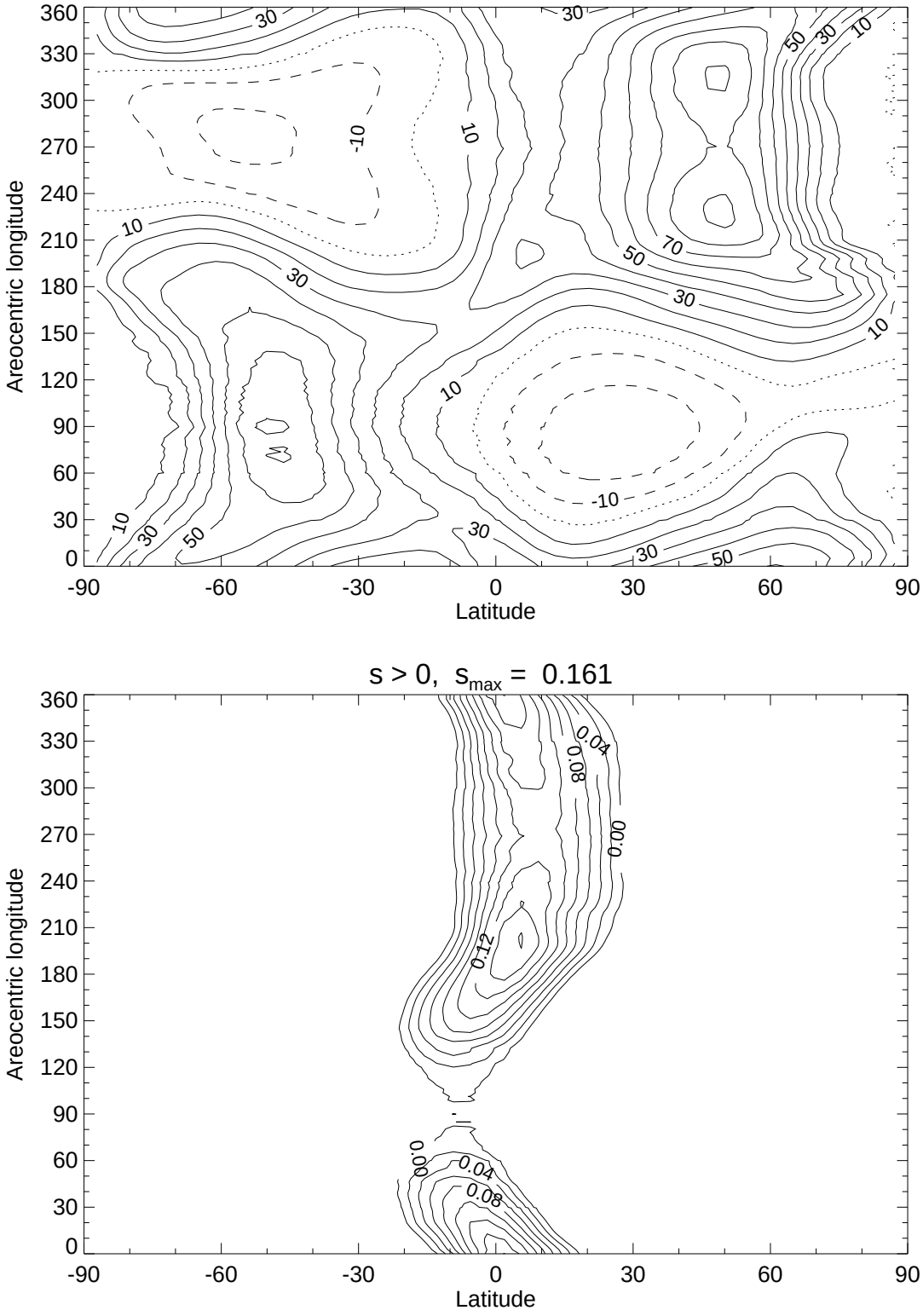

Figure 2. As Fig. 1, but for the Viking×5 dust scenario.

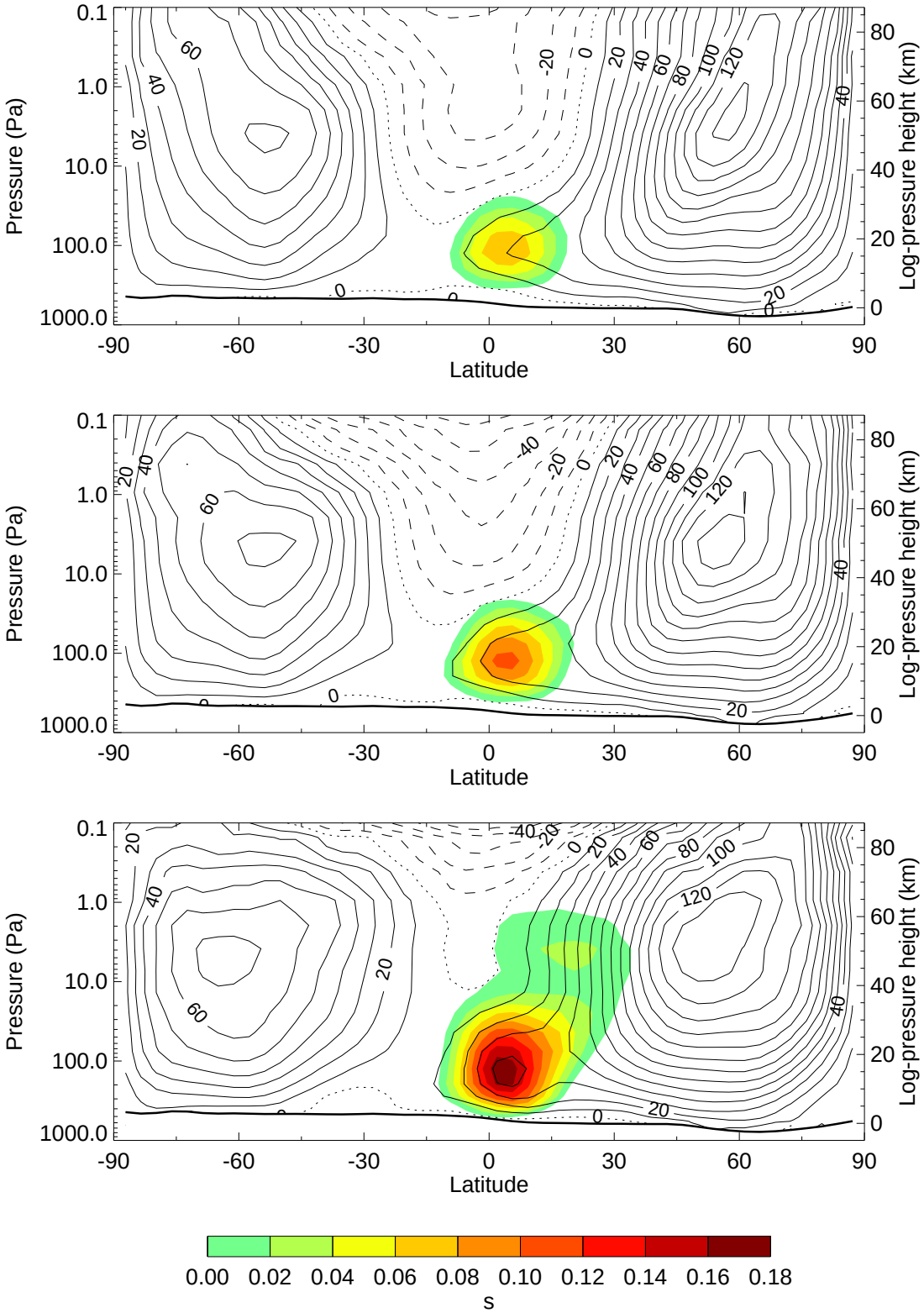

Figure 3. Zonal-mean zonal wind (contours) and local super-rotation index, s (shades), in a model run with Viking (upper panel), Viking$\times$2 (middle panel) and Viking$\times$5 (lower panel) dust scenarios. A time average has been taken over $L_S = 180°$–$210°$, a period following northern autumn equinox. The dust optical depth at 700 Pa, $\tau = 0.73$, 1.45, 3.63, respectively, in the middle of the averaging period (Eqn. 1).

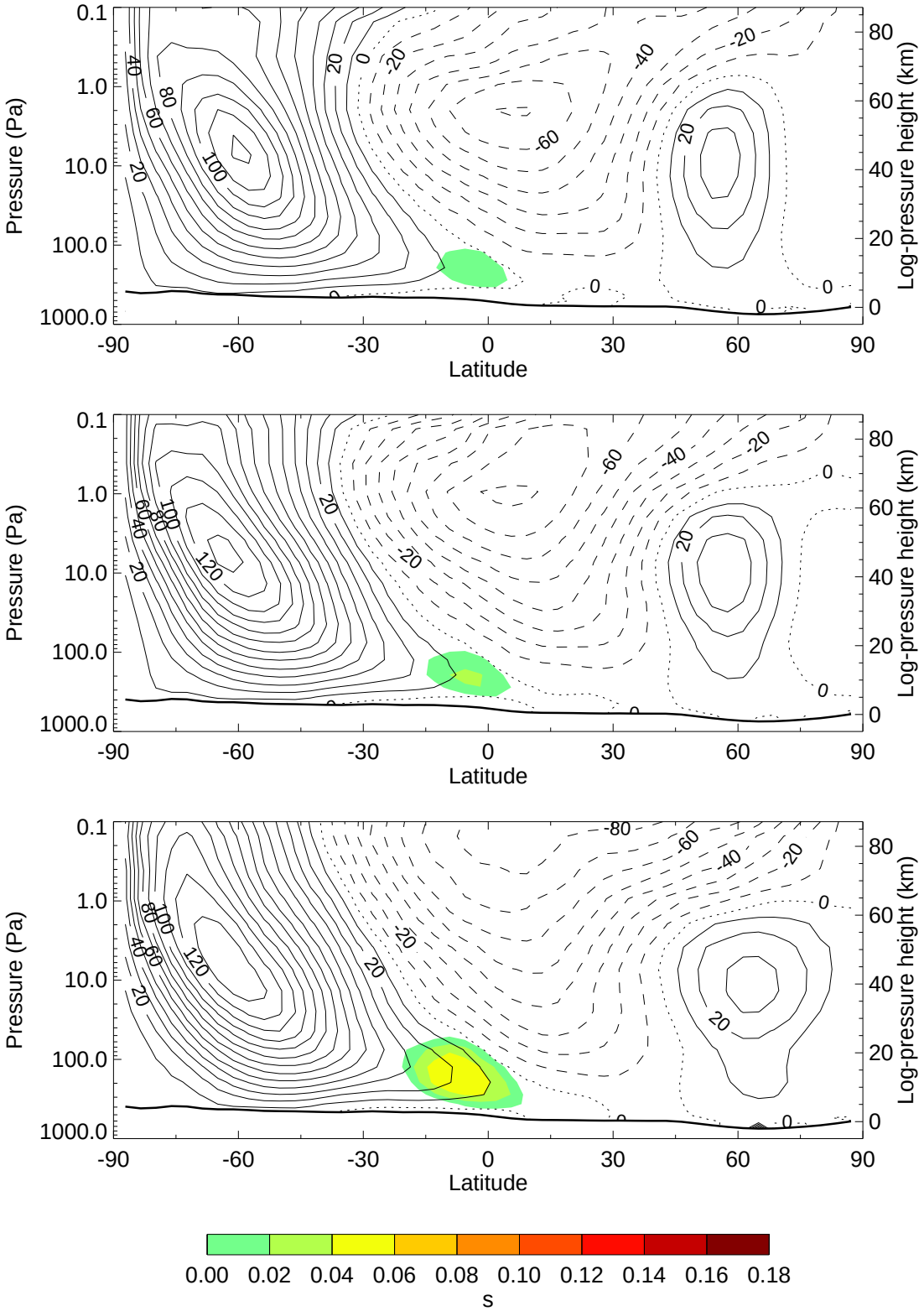

Figure 4. As Fig. 3, but for a northern summer period, $L_S = 120°$–$150°$. The panels show the same three dust scenarios; in the middle of the averaging period, $\tau = 0.45$, 0.91, 2.27, respectively (Eqn. 1).

tends to be dominated by a single cell at most times of year.

The equinoctial regime is transitional, as the atmosphere switches from a northern summer to winter solsticial circulation, with the larger, northern hemisphere (clockwise) cell growing to dominate the cross equatorial circulation as time progresses. The relative strengths of the northern and southern hemisphere cells in Fig. 5 are sensitive to the averaging period chosen. As observed by *Haberle et al.* [1993], the intensity of the Hadley circulation in the model is very sensitive to the sub-solar latitude, where heating is a maximum [*Schneider*, 1983; *Lindzen and Hou*, 1988]. Figure 6 shows the meridional circulation from the northern hemisphere summer period, dominated by a single, anticlockwise cell which grows in intensity with dust loading and circulates around the region of the equatorial jet. A single, dominant Hadley cell, is more typical of the Martian circulation at most times other than close to equinox [e.g., *Haberle et al.*, 1993; *Forget et al.*, 1999].

Tidal forcing

Wilson and Hamilton [1996] describe an experiment in which removing the diurnal cycle from their model resulted in no westerly flow over the equator. In this section, results from a series of similar experiments are described, in which both the diurnal tide and model topography are removed, alone and in combination, to isolate the contribution of tidal components. As noted earlier, non-axisymmetric processes are required to explain super-rotation. The observation that super-rotation in this model increases with dust loading and therefore with increased diurnal forcing indicates the likelihood of tidal forcing being a major factor. Planetary waves might also play a role, but baroclinic waves tend to become weaker at high dust loading as the atmosphere becomes more stably-stratified, in contrast to the strengthening seen in the equatorial jet.

In order to investigate this hypothesis, the present GCM was run again, under Viking×5 dust conditions which would normally lead to a strong westerly jet, but with the solar heating averaged around latitude circles in order to remove the diurnal tide. The amplitude of the various tidal components at one height in a model with a diurnal cycle is illustrated in Fig. 7. The case with both full topography and a diurnal cycle shows strong diurnal, semi-diurnal and higher harmonic components propagating toward the west, and a strong eastward-propagating wavenumber one, Kelvin mode. Without a diurnal cycle (not shown) there are only very weak modes with periods of around one day; these have amplitudes two orders of magnitude smaller than they do in the presence of a diurnal heating cycle.

The zonal wind as a function of latitude and height is

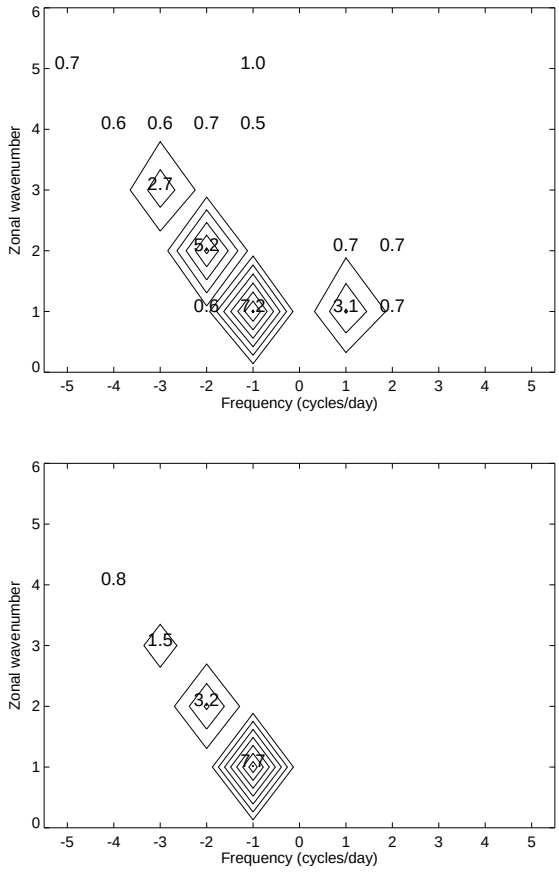

Figure 7. Amplitude spectrum in frequency–zonal wavenumber space of the temperature signal at the equator on the 25 Pa pressure surface (about 32 km altitude) for the Viking×5 scenario with a full diurnal tide. The upper panel shows the results from the full GCM and the lower panel results from a model with no topography and uniform surface properties, but still forced with a diurnal cycle. Negative frequencies correspond to westward propagation. The contour interval is 1 K and modes with amplitudes greater than 0.5 K are labeled.

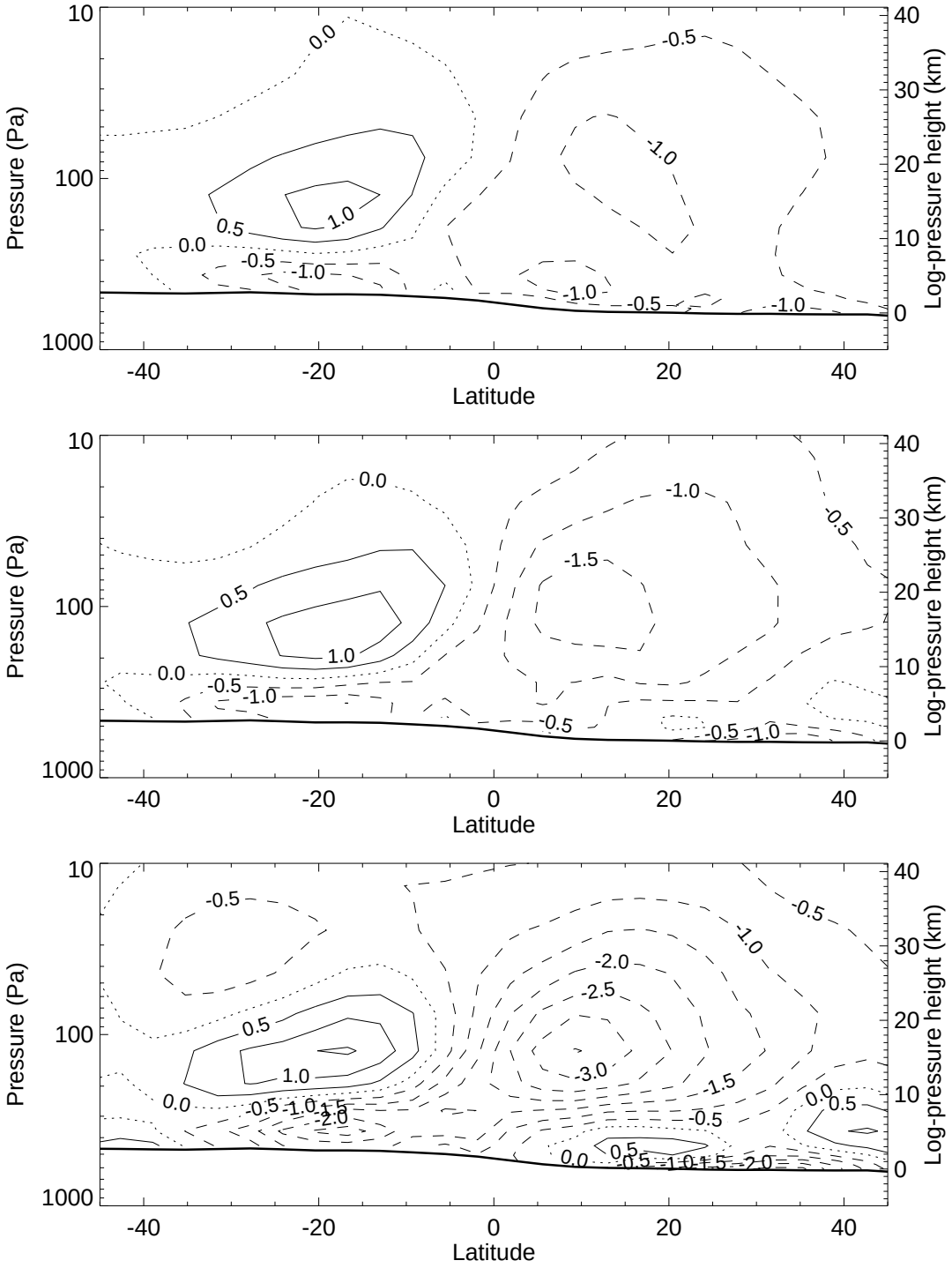

Figure 5. Mean meridional circulation for the three dust scenarios, for the northern autumn equinox period ($L_S = 180°–210°$), corresponding to Fig. 3. Note that the region of the plot only covers half the height and latitude range of previous figures, to focus on the region of interest. Positive streamfunction contours imply anticlockwise circulation in the plane of the figure. Contours are labeled in units of 10^9 kg/s.

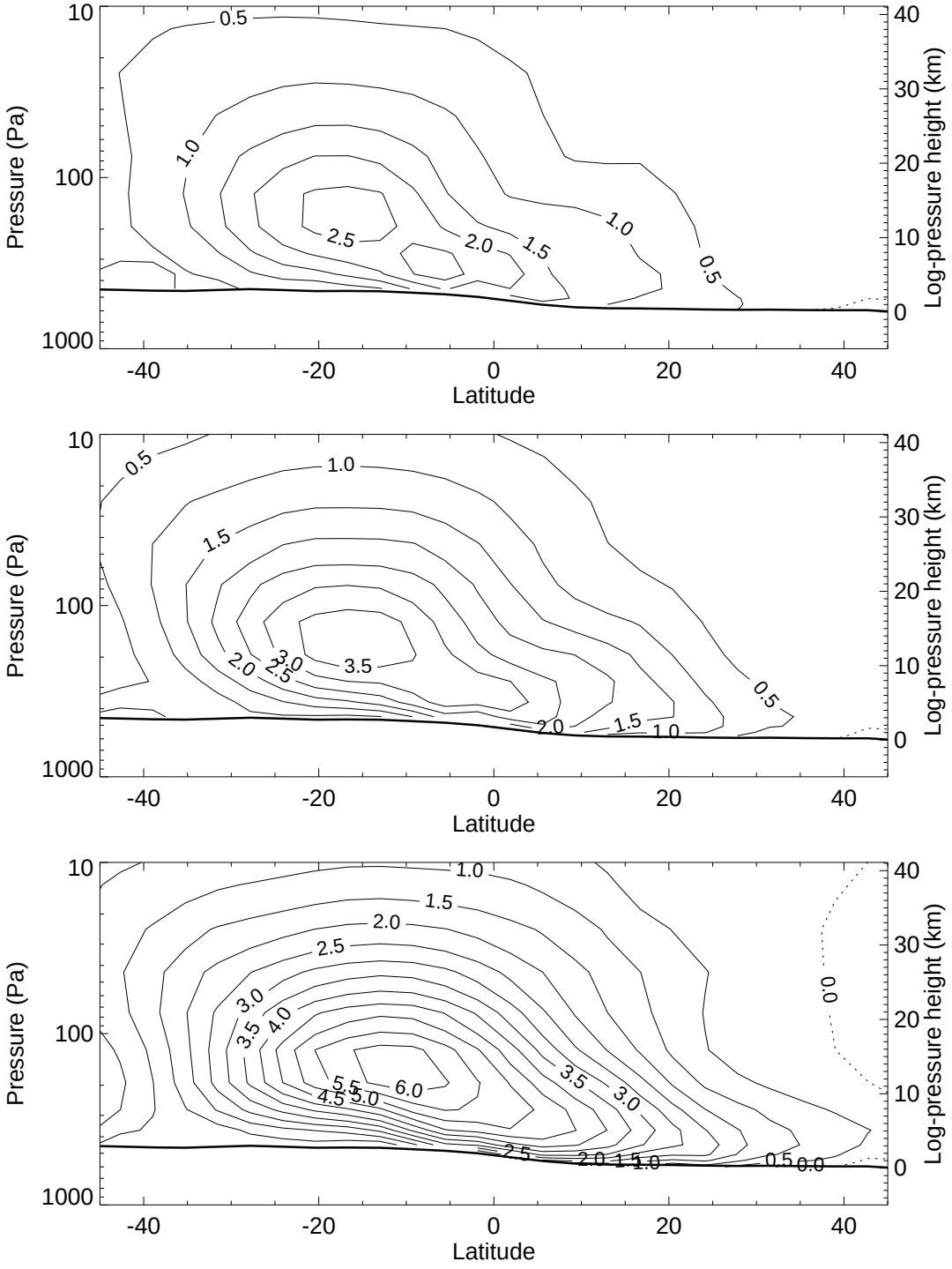

Figure 6. As Fig. 5, but for the northern summer ($L_S = 120°$–$150°$) period, corresponding to Fig. 4. Contours are labeled in units of 10^9 kg/s.

shown in Fig. 8 for experiments both with and without diurnal tides. It is clear that when the diurnal cycle is removed there is no evidence of any super-rotation in the atmosphere below 60 km, in contrast to the distinct westerly flow seen in the presence of a diurnal cycle, confirming the importance of tides in producing this zonal-mean wind [*Wilson and Hamilton*, 1996].

It is important to note that the global atmospheric super-rotation in the case without tides, $S = 0.058$, is the same as that in the case with tides under the same Viking$\times 5$ dust loading conditions, despite the maximum local super-rotation being weaker, $s = 0.100$, and occurring only in the upper atmosphere. The tides can redistribute angular momentum, and create a strong local maximum in the equatorial westerly jet, but do not alter the integrated atmospheric total axial angular momentum.

Large differences are seen in the upper atmosphere of Fig. 8, principally where the mid-latitude westerly jets fail to close with height in the absence of tides and the strong retrograde flow seen high above the equator also disappears without the diurnal cycle. The role that the tides must play in closing the mid-latitude westerly jets is particularly striking and apparently stronger than the effects of transient and stationary planetary waves, present in both simulations.

The absence of a strong easterly, and indeed evidence of prograde westerly flow, in the upper atmosphere of the model without a diurnal cycle is an observation worthy of consideration. Figure 8 shows the flow up to altitudes around 85 km, at which the version of the GCM used for this study becomes less accurate owing to the neglect of non-Local Thermodynamic Equilibrium effects on the radiative budget. The easterly flow in the upper part of these results with a diurnal cycle, however, does not appear to be an artifact of the position of the model top, which is in any case higher than the top of these diagrams at about 100 km altitude. Easterly flow is a robust feature of the GCM which has the top raised to above 120 km, an improved radiation scheme which is more accurate up to this altitude, and an increased number of vertical levels, e.g. 32.

Previous work [*Barnes and Haberle*, 1996; *Wilson and Hamilton*, 1996; *Forget et al.*, 1999] has discussed the presence of easterlies high above the equator and attributed their presence to momentum transport by the cross-equatorial zonal-mean meridional flow. *Wilson* [1997] reported that tides can induce a high-latitude expansion of the Hadley circulation in the winter hemisphere, possibly enhancing the meridional transport. This is indeed an important mechanism when the circulation is in a solsticial state, but the example shown here indicates that direct tidal forcing is also important in producing equatorial easterlies. The GCM with no diurnal cycle does produce easterlies above the equator, by the zonally-symmetric meridional transport mechanism, as it moves into a northern winter solsticial flow regime, but these peak at roughly 100 m/s within the model domain at about 60 km altitude. At the same time of year, the GCM with a diurnal cycle has easterlies peaking at over 200 m/s and increasing with height, into the model sponge layer. The tidal effect seems to be at least comparable with the meridional transport of zonal momentum. This is broadly consistent with the difference seen at equinox, 40 m/s easterlies above 80 km with a diurnal cycle, compared to 20 m/s westerlies without. As can be seen from the zonal-mean meridional circulation close to equinox, Fig. 5, there is little cross-equatorial momentum transport at this time of year and the easterly acceleration in the upper atmosphere may be attributed largely to breaking tides.

Further experiments have been conducted to isolate which tidal modes are most important in forcing the zonal flow. The Viking$\times 5$ scenario has been re-run using a model with no topography and with globally-uniform surface thermal properties (albedo and thermal inertia). The lower panel of Fig. 7 shows clearly the effect on the tidal modes of the removal of variations in surface topography and thermal properties. As noted earlier, the interaction of solar forcing and surface inhomogeneities may give rise to a variety of non-sun synchronous responses, e.g. interaction of the diurnal tide with zonal wavenumber two topography may generate a diurnal period, zonal wavenumber one Kelvin mode. Without such interactions, there are no large, eastward-propagating Kelvin modes, and a simpler structure in the westward sun-synchronous tides, with a diurnal, semi-diurnal and higher harmonic components only.

Figure 9 compares the zonal winds from experiments with the smooth surface, both with and without a diurnal cycle, as in Fig. 8 for the full model. The super-rotating jet produced with a diurnal cycle is even stronger than that in the GCM with full Mars topography and thermal properties. Westerly wind speeds peak at around 70 m/s about 10 km above the surface at the equator and local super-rotation reaches peak values around $s = 0.30$, compared to $s = 0.16$ in the case with full topography.

We therefore conclude that the primary driving force for the westerly jet in the lower atmosphere is a momentum flux induced by the sun-synchronous, westward-propagating diurnal tide. The generation of an eastward Kelvin mode may indeed have the opposite effect on the mean flow, with a relative reduction in the amplitude of the westerly zonal winds.

Comparison of Figs. 8 and 9 confirms the role that tides play in closing the westerly jets in the upper atmosphere, although it is clear that the jets are most strongly closed in the full case in the presence of both sun-synchronous tides, Kelvin modes and stationary waves from full topography.

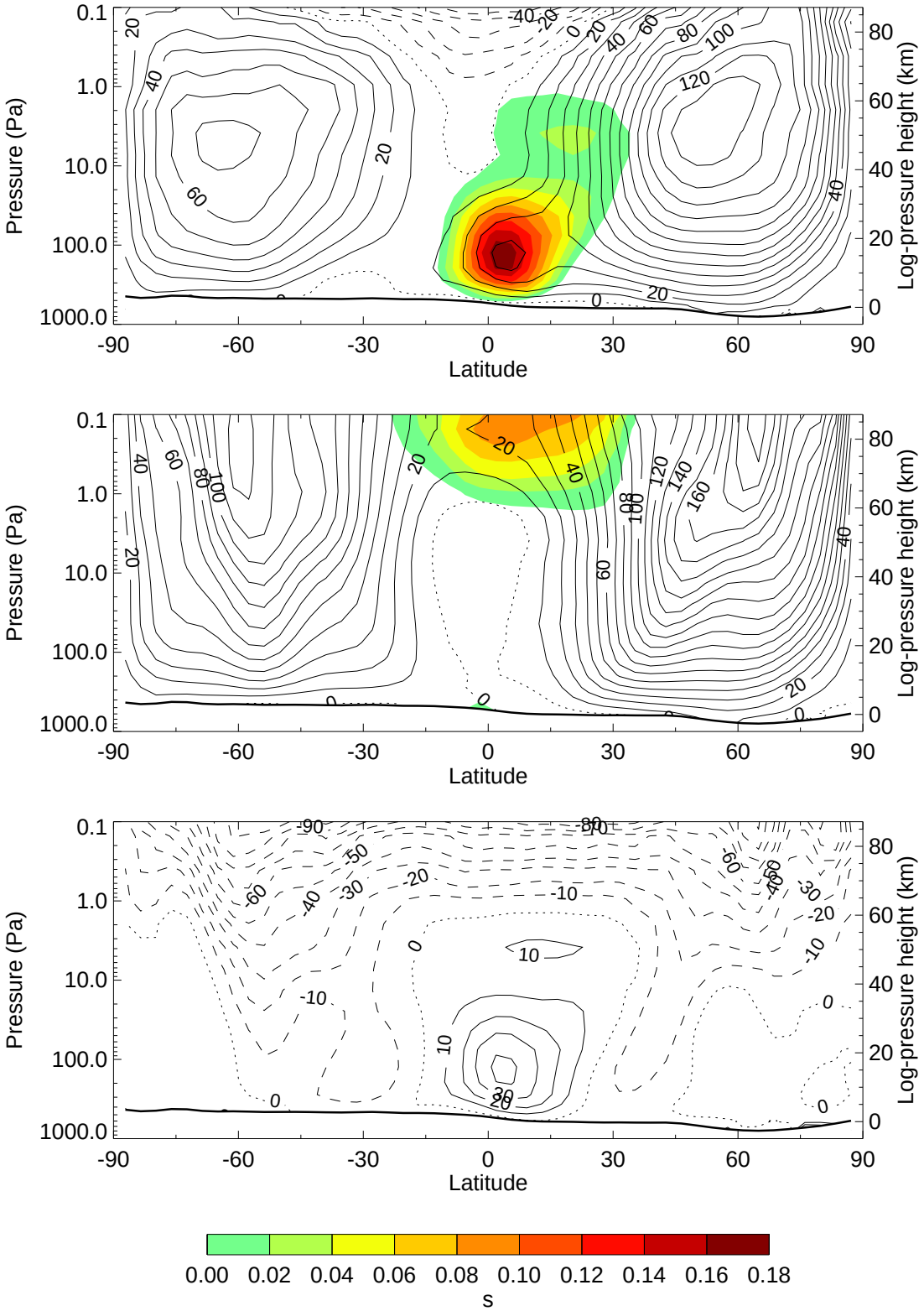

Figure 8. Comparison of the zonal-mean zonal wind in a model run with the normal diurnal cycle (upper panel), one with diurnally-averaged insolation (middle panel) and the difference between them (lower panel). Regions in which $s > 0$ are shaded. Both use the Viking×5 dust scenario and a time average has been taken following northern autumn equinox, $L_S = 180°$–$210°$.

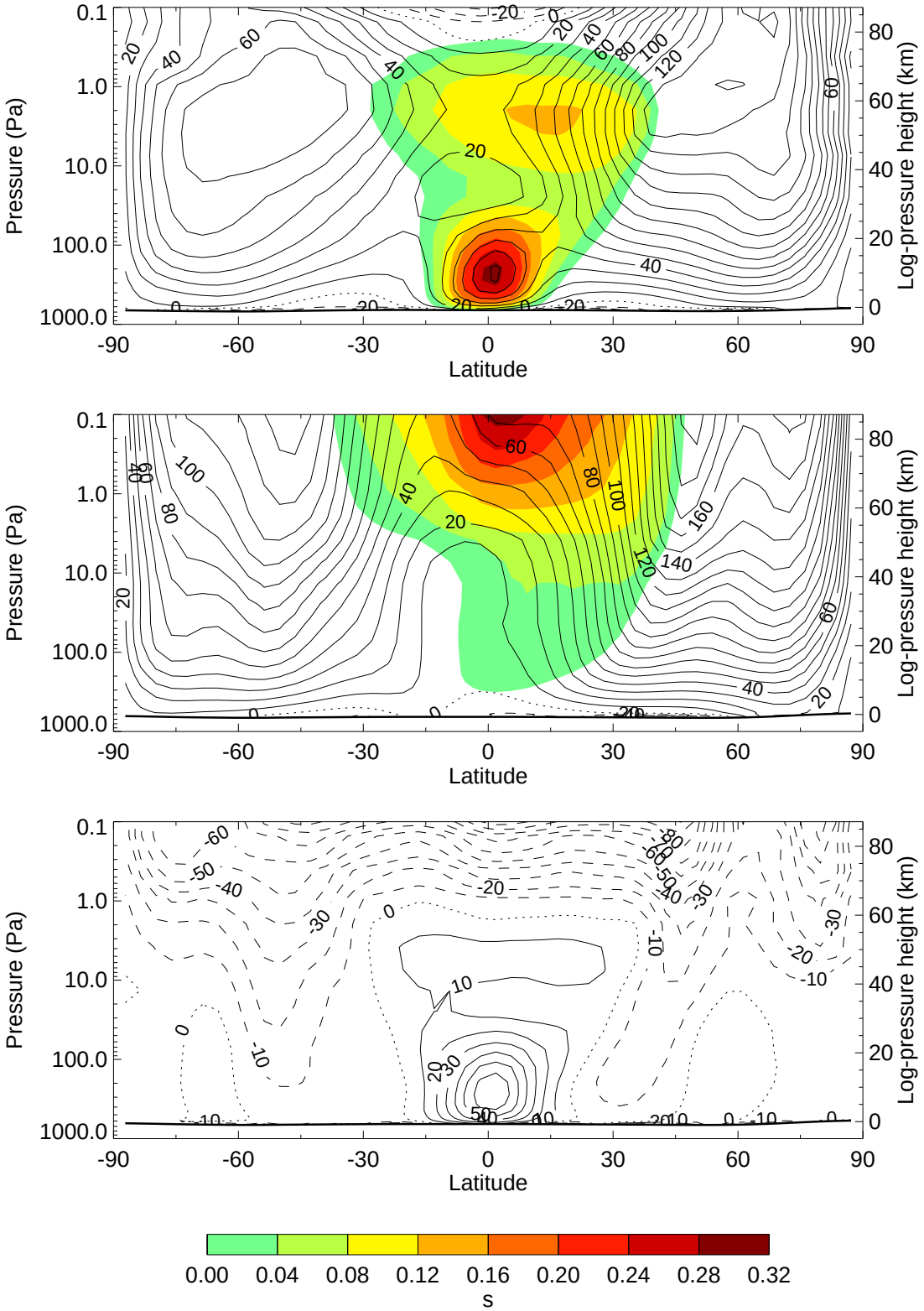

Figure 9. Comparison of the zonal-mean zonal wind in a model run with smooth topography and surface properties, with the normal diurnal cycle (upper panel), one with diurnally-averaged insolation (middle panel) and the difference between them (lower panel). Regions in which $s > 0$ are shaded with an interval of 0.04, twice that of Fig. 8. Both use the Viking×5 dust scenario and a time average has been taken following northern autumn equinox, $L_S = 180°$–$210°$.

The local super-rotation in the upper atmosphere of the model without a diurnal cycle must be attributable to an eddy process other than atmospheric tides, since waves with periods of a day or less are almost absent. The most likely candidates are planetary waves. Model diffusion may also play a role in transporting momentum equatorward from the mid-latitude westerly jets, but in this case the upper atmosphere seems relatively insensitive to reducing the weak, highly scale-selective sub-grid scale diffusion parameter in the spectral model. Both transient and stationary planetary waves are able to propagate to high levels in this model, where the westerly flow in the mid-latitude jets remains strong with increasing height, Fig. 8. Transient waves appear to make the largest contribution, confirmed by results from a model with no diurnal cycle or topography, Fig. 9, and hence no strong stationary waves. In this case the local super-rotation in the upper atmosphere is particularly intense, as is the baroclinic wave activity, also responsible for the splitting of the northern hemisphere westerly jet into two distinct maxima at upper levels.

Figure 10 shows the zonal mean temperature state from the full GCM experiments with and without a diurnal cycle, shown in Fig. 8. While the upper atmosphere is significantly different, with much stronger latitudinal gradients in the presence of diurnal tides in balance with the closure of the westerly jets with height, there is remarkably little difference in the temperature structure below about 50 km altitude, except over the poles. Very similar patterns of temperature differences are seen in the experiments with smooth topography, Fig. 9. This highlights a generic difficulty in relying upon thermal observations to confirm the presence of a westerly jet close to the equator, where gradient wind balance breaks down [*Andrews et al.*, 1987].

The results presented here are in accordance with the predictions of *Fels and Lindzen* [1974], made with a linearized model of internal gravity waves, for the effects of thermally excited gravity waves on Earth and Venus. Westerly (eastward) winds are induced in the region in which westward thermal tides are generated, in the lower atmosphere, with the region of maximum solar heating moving upward in the atmosphere as the dust optical depth increases. Conversely, easterly (westward) zonal winds are generated in the upper atmosphere where the tides break and dissipate their momentum.

Eliassen-Palm flux diagnostics

The following figures show the Eliassen-Palm (EP) flux and the pattern of EP flux divergence, which represents the stress acting on the zonal momentum owing to wave-mean flow interaction [*Andrews et al.*, 1987], from the GCM experiments described earlier. Two different periods are shown, northern autumn equinox ($L_S = 180°$–$210°$), when the equatorial westerly jet is large and steady, and mid-late northern summer ($L_S = 120°$–$150°$), when the jet is growing rapidly, as in Figs. 3 and 4.

Figures 11 and 12 contour the tendency to the zonal momentum equation resulting from the EP flux divergence ($-\nabla \cdot \mathbf{F}/a\cos(\phi)$, where $\nabla \cdot \mathbf{F}$ is the EP flux divergence, a the radius of Mars and ϕ the latitude), rescaled into units of m/s/day for convenience. In each case the EP flux was calculated from fields stored twelve times per day in the $30°$ areocentric longitude period (50 and 60 Mars days respectively) and then averaged together. EP flux vectors, $\mathbf{F}$, are also shown, scaled for plotting on a log-pressure axis following the conventions established in *Edmon, Jr. et al.* [1980], although the EP flux here includes ageostrophic terms since the diagnostics are required near the equator,

$$\mathbf{F} = a\cos\phi\left[\overline{v'u'} - \overline{u}_p\frac{\overline{v'\theta'}}{\overline{\theta}_p}, \right.$$
$$\left.\overline{\omega'u'} + \left\{\frac{(\overline{u}\cos\phi)_\phi}{a\cos\phi} - 2\Omega\sin\phi\right\}\frac{\overline{v'\theta'}}{\overline{\theta}_p}\right], \quad (7)$$

where $\overline{x}$ and x' denote the zonal mean and eddy component of x respectively. The sign convention for EP flux used here should be noted as following *Andrews and McIntyre* [1978] and *Read* [1986a], the opposite to that often used, e.g. *Andrews et al.* [1987]. The reason for this is to emphasize the direction of momentum transport by the eddies, primarily through the $\overline{v'u'}$ term, by the direction of the vectors plotted.

In the equinoctial case the EP flux divergence is actually very small in the region where the jet is large and forms a quadrupole pattern around the jet, somewhat reminiscent of the EP flux divergence shown by *Hamilton* [1982] for a high dust case, although the magnitude of the divergence is smaller in the present case. The amount of dust, and its radiative effect, is not necessarily comparable in each case. *Zurek* [1986] also found smaller divergences than *Hamilton* [1982] as a result of differences in the dust optical properties assumed. It should also be noted that the *Hamilton* [1982] example was for a solsticial case, Fig. 11 is equinoctial. This implies a small contribution from the EP flux divergence to the westerly equatorial jet, but over this period the amplitude of the jet is indeed fairly steady.

A perhaps more illuminating period is shown in Fig. 12, when the jet is continuously growing during the averaging period. At this time there are significant regions of positive convergence lying directly in the region where the jet appears, with amplitudes of more than 5–10 m/s/day, according to dust loading. Averaged over a 60 day period, these

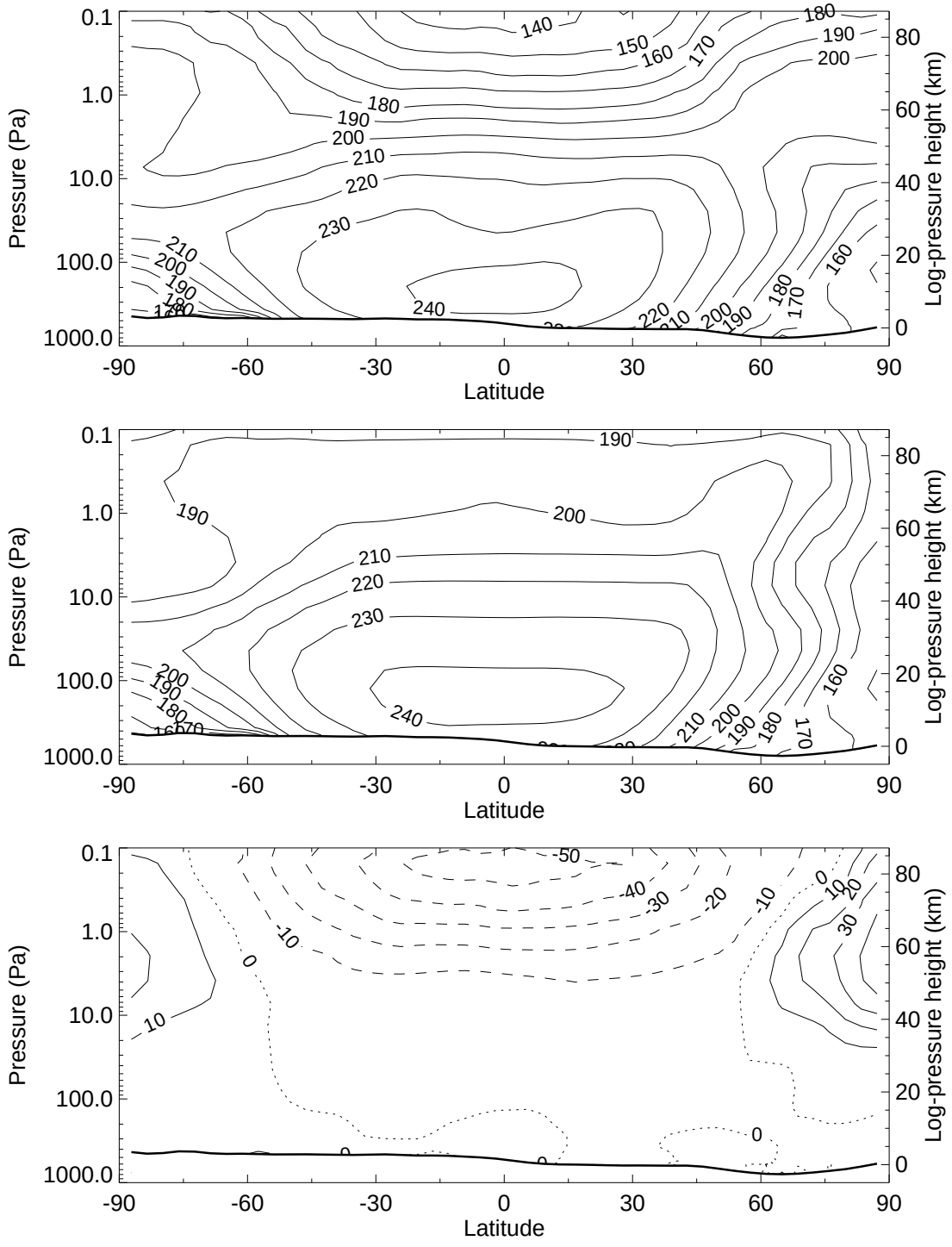

Figure 10. Comparison of the zonal-mean model temperatures corresponding to the zonal winds shown in Fig. 8.

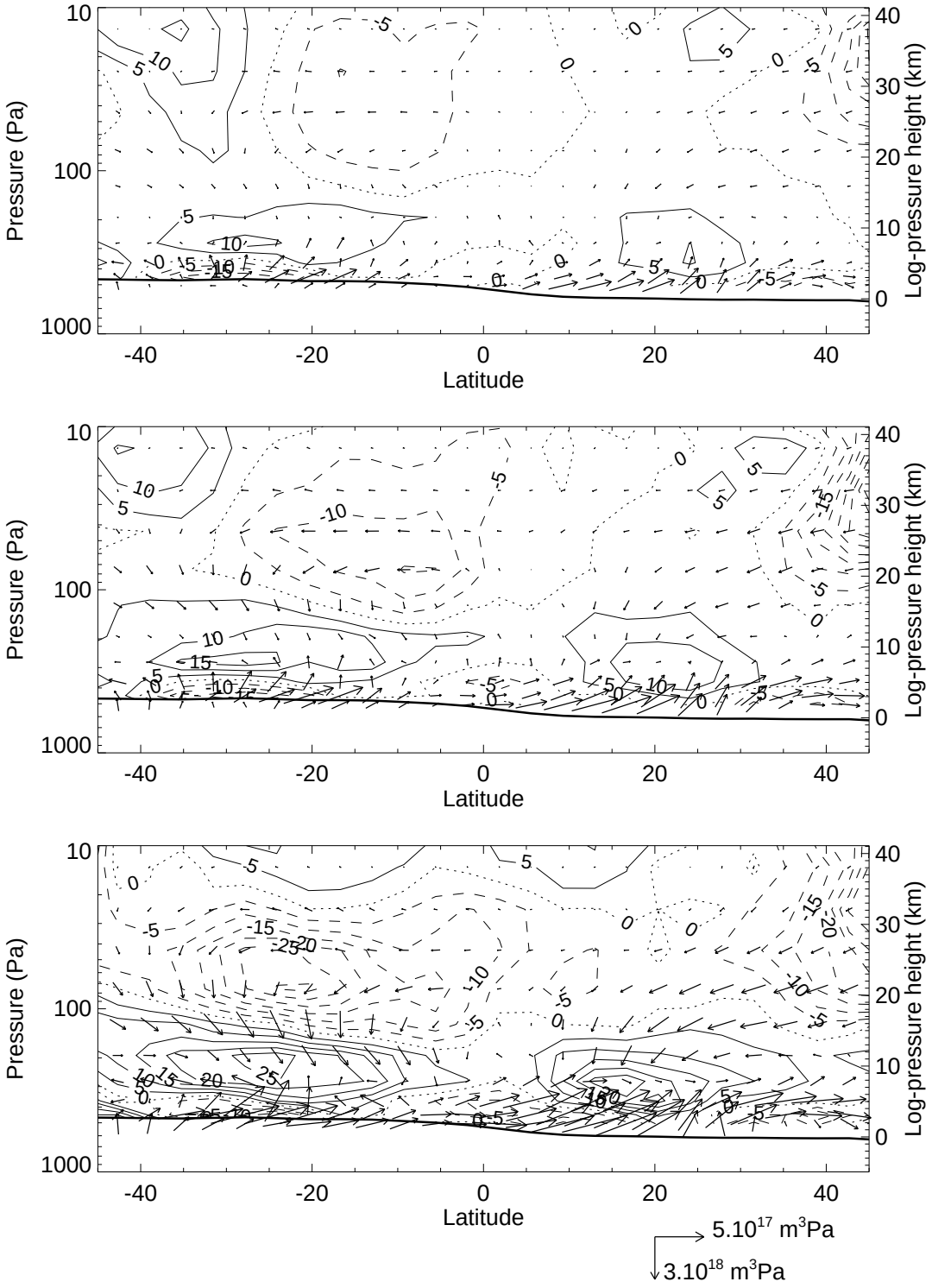

Figure 11. The tendency for the zonal momentum equation resulting from the EP flux divergence following northern autumn equinox ($L_S = 180°$–$210°$), shown as contours (m/s/day), with the EP flux vectors and a scale arrow indicated. Definitions of terms are given in the text. Note that the region of the plot only covers half the height and latitude range, as in Fig. 5. The panels show the three dust scenarios, ordered as in Fig. 3.

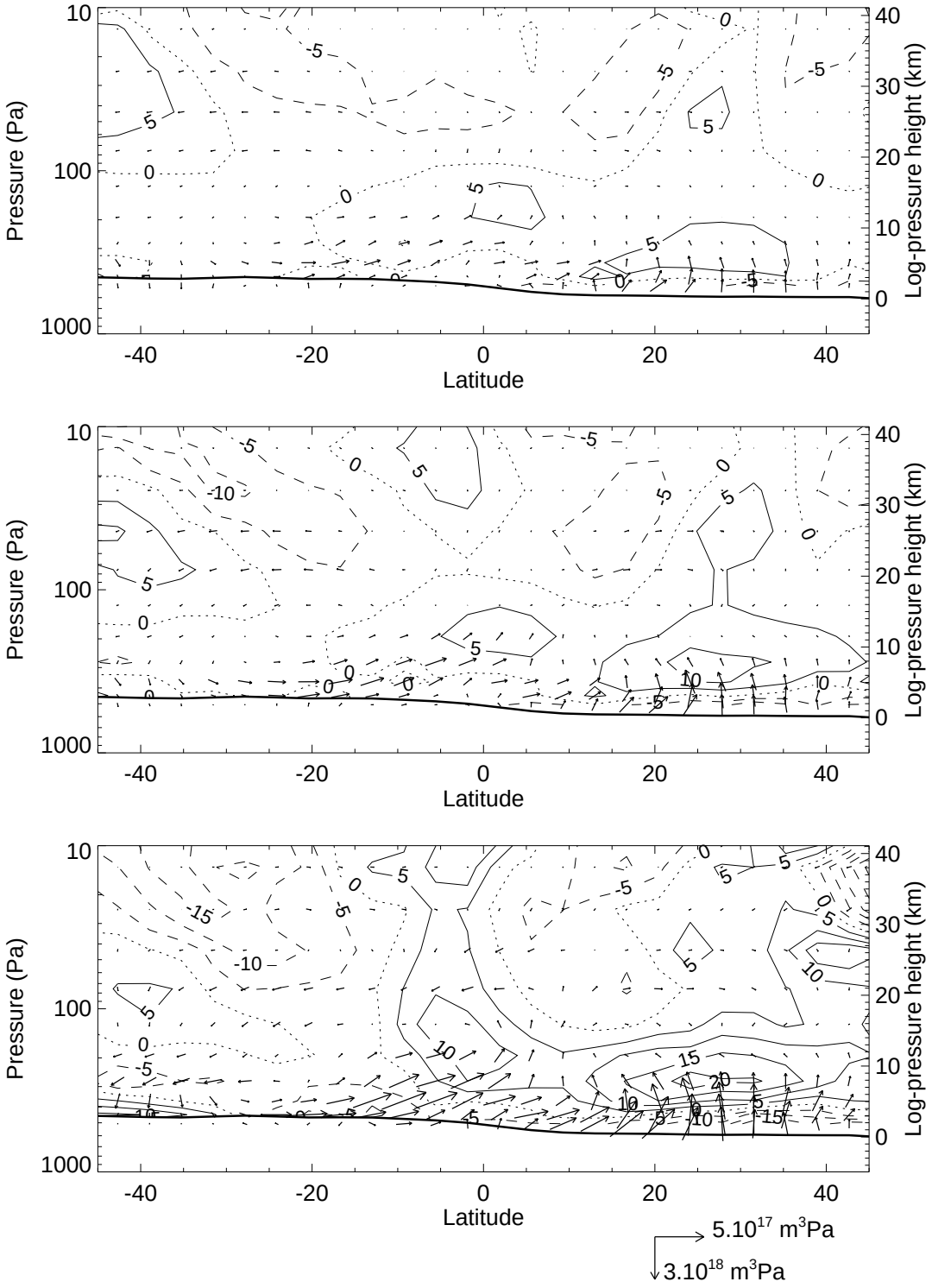

Figure 12. As Fig. 11, but for the northern summer ($L_S = 120°$–$150°$) period. The panels show the three dust scenarios, ordered as in Fig. 4.

are more than large enough to account for the growth of the super-rotating jet, if not entirely balanced by meridional transport or friction. The EP vectors indicate that the main contribution is a flux of westerly momentum from the southern (winter) hemisphere, where there is a large prograde jet, see Fig. 4.

A strong region of EP flux convergence can also be seen around 20°–30°N, below 10 km altitude in Fig. 12; a counterpart to regions distributed more symmetrically about the equator in Fig. 11. This is a region close to the sub-solar latitude and at a height where the diurnal sun-synchronous tide is being most strongly forced in the summer hemisphere. Westerly zonal momentum is induced in a region where westward-propagating tides are forced [*Fels and Lindzen*, 1974]. The strong westerly accelerations implied here are partly balanced by advection of easterly momentum in the rising branch of the Hadley Cell, see Fig. 6, but this is also a region which is undergoing a transition from easterly flow of 20 m/s to weak westerly flow by the end of the averaging period ($L_S = 120°$–$150°$) and thereafter becomes strongly westerly, see Fig. 2.

In order to help to isolate the role of the tidal components in the EP flux, Fig. 13 compares the tendency and EP flux vectors in northern hemisphere summer for Viking×5 dust scenarios both with and without a diurnal cycle imposed (see Fig. 8). These show clearly that the main regions of EP flux convergence, and so westerly forcing, in the lower, equatorial atmosphere are indeed induced by tidal components and are absent in the experiment with diurnally-averaged insolation which has no low-level equatorial westerly jet.

The tendencies resulting from the EP flux divergence should be viewed together with the transport by the residual mean meridional circulation, the Eulerian mean meridional circulation corrected for the component balanced by mean large-scale eddy transport [e.g., *Andrews et al.*, 1987]. The residual mean circulation cannot transport angular momentum up-gradient steadily to maintain a prograde jet, but the effects of transport are combined with the EP flux divergence to find the total tendency on the zonal momentum equation. The residual mean meridional circulation in the equatorial region is almost identical to the zonal-mean meridional circulation, shown in Figs. 5 and 6. Close to equinox, the residual mean advection tends to balance the small EP flux divergence in the equatorial region, shown in Fig.11. This is consistent with the observation that the strong westerly jet at the equator is almost steady over this period, although away from the equator the zonal mean flow is changing as the northern hemisphere moves into a winter, westerly state. Corresponding diagrams for the period when the jet is growing in northern summer are shown in Fig. 6. In this case, the larger Hadley circulation surrounds the region of interest and actually makes a relatively small contribution to the total zonal momentum tendency at the location of the equatorial jet; this is mainly in the form of a deceleration via the vertical advection of easterly momentum from nearer the surface. Thus the large EP flux divergence tendencies, seen in Fig. 12 at about 10-15 km altitude over the equator, seem to be primarily responsible for forming the super-rotating equatorial jet.

Discussion

Local super-rotation has been mapped in a Mars GCM throughout the Martian annual cycle and as a function of dust loading. It is found to be more pronounced under conditions of higher dust opacity and at equinox, although it is still a significant component of the circulation at other times. In agreement with some previous work [*Wilson and Hamilton*, 1996], thermal tidal modes have been identified as the driving mechanism and, in particular, the main westward-propagating diurnal tide plays the principal role. A pattern of westerly flow at the altitudes where the tides are generated and easterly flow at higher altitudes, where they dissipate, is in accordance with the mechanism proposed by *Fels and Lindzen* [1974]. The degree to which the tides are responsible for easterly flow high above the Martian equator, by an amount comparable with the meridional advection at solstice and as the sole factor at equinox, has not been recognized before. Future work with a GCM with a top raised to above 120 km, and with an improved radiation scheme appropriate to such low pressures, can investigate this further, although the problem becomes complicated by the introduction of CO_2 heating and hence a second thermal forcing region in the upper atmosphere.

The global super-rotation, S, observed in the Mars GCM is approximately a factor of three greater than that estimated for the Earth by *Read* [1986a]. *Read* [1986b] has identified S with a form of Rossby number, $V/\Omega a$, based on a typical flow speed V and planetary radius a. These results are broadly consistent with such an interpretation: Ω is similar for both planets, whereas the radius of Mars is about half that of the Earth and typical wind speeds on Mars are somewhat greater.

It is worthy of particular note that the global super-rotation, S, for the Mars GCM increases only slowly with dust loading (which leads to an increase in the mean wind speed), and is insensitive to the details of how the super-rotation is caused and where it is positioned in the atmosphere; simulations with and without thermal tides under the same dust conditions give similar values of S. This behavior is in marked contrast to the local super-rotation, s, which is strongly dependent on dust loading and on the mechanism

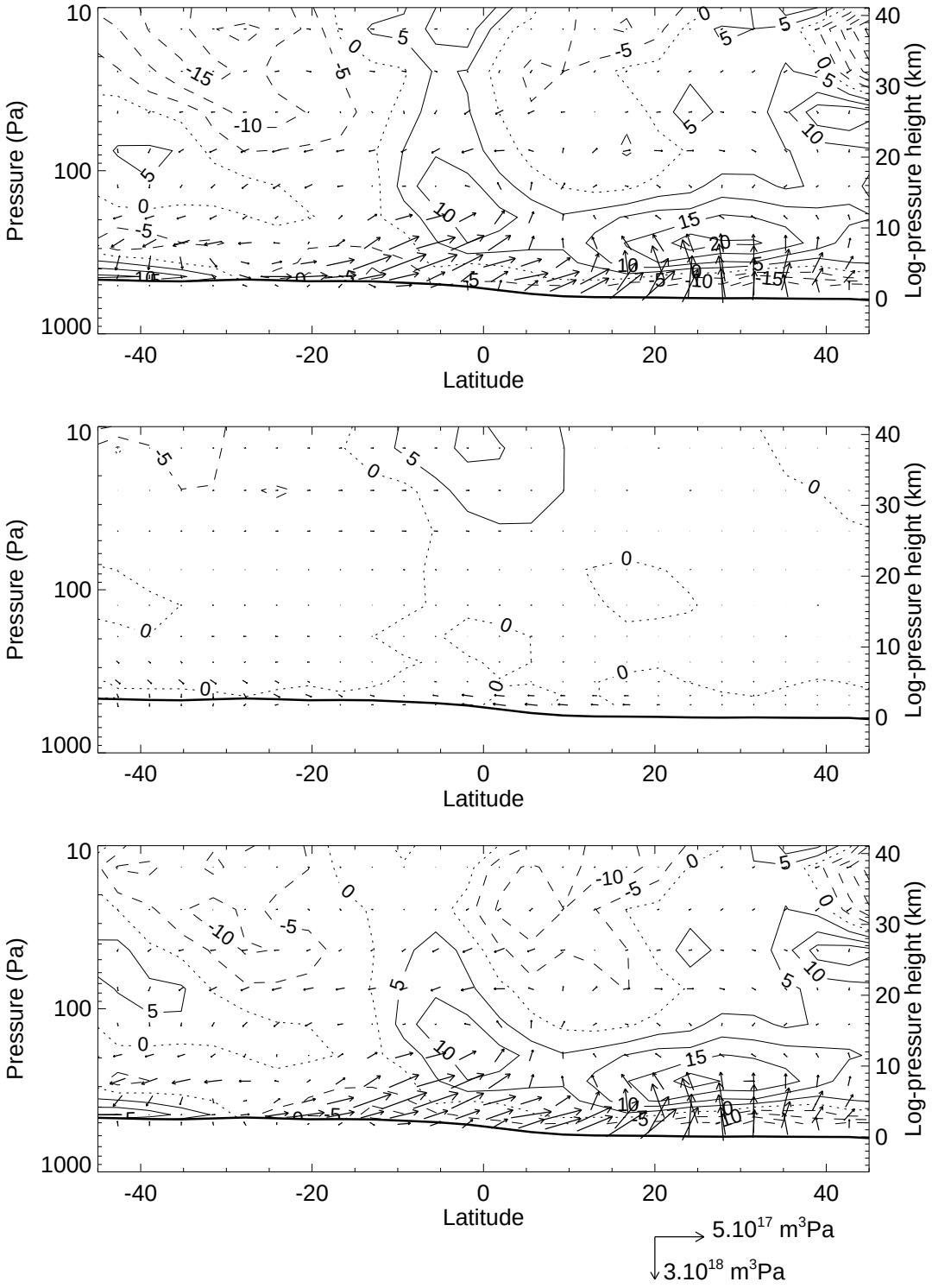

Figure 13. Comparison of the tendency for the zonal momentum equation resulting from the EP flux divergence for an experiment with the normal diurnal cycle (upper panel), one with diurnally-averaged insolation (middle panel) and the difference between them (lower panel). The period covered is northern hemisphere summer ($L_S = 120°$–$150°$), with the tendency (m/s/day) and the EP flux vectors shown as in Fig. 12. Both use the Viking$\times 5$ dust scenario.

which leads to its generation.

The Earth can also exhibit local super-rotation, both in the upper troposphere as a result of Rossby wave forcing and, most prominently, in the stratosphere during the westerly phase of QBO, which is most likely forced by a combination of internal gravity and Kelvin waves [*Andrews et al.*, 1987]. The peak westerly equatorial winds seen in the QBO are about 20 m/s at around 25 km altitude, and such strong winds do not occur on every cycle. From Eqns. 4 and 6, this allows an estimate of the maximum local super-rotation, $s \approx 0.04$ with terrestrial parameters. This is smaller than the peak values of s found for Mars by a factor of almost two under moderate dust conditions, and by a factor of four when the Martian atmosphere is dusty.

Both local and global super-rotation require angular momentum transfers by eddy processes which must act up-gradient with respect to the zonal-mean gradient of angular momentum. On Earth, such up-gradient transfers are relatively weak. Near the equator, tropical convection has the effect of mixing angular momentum [*Emanuel*, 1994] and suppressing development of super-rotation in the lower troposphere. In the terrestrial upper troposphere and stratosphere, gravity, Kelvin and Rossby waves may break and give rise to a stress on the zonal-mean flow, with the possibility of super-rotation as described above. The diurnal thermal tide is much stronger on Mars than it is on Earth and, as shown here, can transport angular momentum up-gradient more easily, resulting in the strong super-rotation seen in the Mars GCM. The super-rotation peaks at equinox, as the solar forcing becomes symmetric about the equator, strongly forcing the direct, diurnal thermal tide in the equatorial region. EP flux divergences indicate a westward forcing over the equator throughout a long period prior to equinox as the westward equatorial flow is accelerated.

The detection of a low-level equatorial westerly flow on Mars by conventional remote-sounding mechanisms would be extremely difficult. The jet has very little signature in terms of temperature, as illustrated in Fig. 10, and is most prominent under high dust conditions, when infrared remote soundings are most difficult to retrieve. There is a potential role for microwave observations, which are less hindered by high dust opacities, and can potentially derive winds through Doppler shifts, although it is not clear that it would be possible to measure winds sufficiently accurately at altitudes below 30 km.

Another possible means from remote sensing would be detection via tracking inhomogeneous tracers, in particular dust or water clouds, which may be concentrated in the lower part of the atmosphere and which may be advected eastwards by an equatorial jet. In order to do this, not only would longitudinal asymmetries be required in order to track features, but it would be necessary to resolve the tracer in the vertical. This is because there is a region of easterly flow immediately above the surface at the equator, as a result of torque balance between the atmosphere and the surface, given westerlies in mid-latitudes. A super-rotating westerly does not take over until between about half and one pressure scale heights above the zonal-mean surface; equally, a large part of the atmosphere above the westerly jet has strong easterly winds (Figs. 3 and 4). Hence both a significant mass and volume fraction of the atmosphere will be moving westward and it would not be possible to detect the eastward jet using observations of a tracer which were not resolved in the vertical. In situ wind measurements, e.g. from entry probes, may be one possible technique for unambiguous detection of westerly flow in future.

The prospects for tracking high-level easterly winds, and using these to calibrate the model, may be better using remote-sensing techniques. There are already Earth-based microwave measurements which imply strong, $>$100 m/s, easterly winds in the Martian middle atmosphere at about 50–80 km altitude [*Lellouch et al.*, 1992], although these are subject to large uncertainties. Similar techniques from a microwave instrument aboard an orbiting spacecraft could be subject to smaller errors, have improved height resolution and provide coverage throughout the Martian seasonal cycle.

Acknowledgments. We are grateful for the support during this work from the UK Particle Physics and Astronomy Research Council. We thank Dr. M. Collins for discussion in the early stages of this work.

References

Andrews, D. G., and M. McIntyre, Generalized Eliassen-Palm and Charney-Drazin theorems for waves on axisymmetric mean flows in compressible atmospheres, *J. Atmos. Sci.*, *33*, 2031–2048, 1978.

Andrews, D. G., J. R. Holton, and C. B. Leovy, *Middle Atmosphere Dynamics*, Academic Press, Orlando, Fl, 1987.

Barnes, J. R., and R. M. Haberle, The Martian zonal-mean circulation: Angular momentum and potential vorticity structures in GCM simulations, *J. Atmos. Sci.*, *53*, 3143–3156, 1996.

Chapman, S., and R. S. Lindzen, *Atmospheric Tides*, Reidel, Dordrecht, Netherlands, 1970.

Edmon, Jr., H. J., B. J. Hoskins, and M. E. McIntyre, Eliassen-Palm cross sections for the troposphere, *J. Atmos. Sci.*, *37*, 2600–2616, 1980.

Emanuel, K. A., *Atmospheric Convection*, Oxford University Press, Oxford, UK, 1994.

Fels, S. B., and R. S. Lindzen, The interaction of thermally excited gravity waves with mean flows, *Geophys. Fluid Dyn.*, *6*, 149–191, 1974.

Forget, F., F. Hourdin, R. Fournier, C. Hourdin, O. Talagrand, M. Collins, S. R. Lewis, P. L. Read, and J.-P. Huot, Improved general circulation models of the Martian atmosphere from the surface to above 80 km, *J. Geophys. Res.*, *104*, 24,155–24,176, 1999.

Gierasch, P. J., Meridional circulation and the maintenance of the Venus atmospheric rotation, *J. Atmos. Sci.*, *32*, 1038–1044, 1975.

Gierasch, P. J., Waves in the amosphere of Venus, *Nature*, *328*, 510–512, 1987.

Gierasch, P. J., et al., The general circulation of the Venus atmosphere: An assessment, in *Venus II*, edited by S. W. Bougher et al., pp. 459–500, Univ. of Ariz. Press, Tucson, 1997.

Haberle, R. M., J. B. Pollack, J. R. Barnes, R. W. Zurek, C. B. Leovy, J. R. Murphy, H. Lee, and J. Schaeffer, Mars atmospheric dynamics as simulated by the NASA/Ames general circulation model, 1, The zonal-mean circulation, *J. Geophys. Res.*, *98*, 3093–3123, 1993.

Hamilton, K., The effect of Solar tides on the general circulation of the Martian atmosphere, *J. Atmos. Sci.*, *39*, 481–485, 1982.

Hide, R., Dynamics of the atmospheres of the major planets with an appendix on the viscous boundary layer at the rigid bounding surface of an electrically-conducting rotating fluid in the presence of a magnetic field, *J. Atmos. Sci.*, *26*, 841–853, 1969.

Hou, A. Y., and B. F. Farrell, Super-rotation induced by critical level absorption of gravity waves on Venus: An assessment, *J. Atmos. Sci.*, *47*, 1894–1901, 1987.

Hourdin, F., F. Forget, and O. Talagrand, The sensitivity of the Martian surface pressure to various parameters: A comparison between numerical simulations and Viking observations, *J. Geophys. Res.*, *100*, 5501–5523, 1995.

Lellouch, E., J. Rosenqvist, J. J. Goldstein, S. W. Bougher, and G. Paubert, First absolute wind measurements in the middle atmosphere of Mars, *Astrophys. J.*, *383*, 401–406, 1992.

Leovy, C. B., Zonal winds near Venus' cloud top level: An analytic model of the equatorial wind, *Icarus*, *69*, 193–201, 1987.

Lewis, S. R., M. Collins, P. L. Read, F. Forget, F. Hourdin, R. Fournier, C. Hourdin, O. Talagrand, and J.-P. Huot, A Climate Database for Mars, *J. Geophys. Res.*, *104*, 24,177–24,194, 1999.

Lindzen, R. S., The application and applicability of terrestrial atmospheric tidal theory to Venus and Mars, *J. Atmos. Sci.*, *27*, 536–549, 1970.

Lindzen, R. S., and A. Y. Hou, Hadley circulations for zonally-averaged heating centered off the equator, *J. Atmos. Sci.*, *45*, 2416–2427, 1988.

Read, P. L., Super-rotation and diffusion of axial angular momentum: I. 'speed limits' for axisymmetric flow in a rotating cylindrical fluid annulus, *Quart. J. Roy. Meteor. Soc.*, *112*, 231–251, 1986a.

Read, P. L., Super-rotation and diffusion of axial angular momentum: II. a review of quasi-axisymmetric models of planetary atmospheres, *Quart. J. Roy. Meteor. Soc.*, *112*, 253–272, 1986b.

Schneider, E. K., Martian great dust storms: Interpretive axially symmetric models, *Icarus*, *55*, 302–331, 1983.

Wilson, R. J., A general circulation model simulation of the Martian polar warming, *Geophys. Res. Lett.*, *53*, 1290–1326, 1997.

Wilson, R. J., Evidence for diurnal period Kelvin waves in the Martian atmosphere from MGS TES data, *Geophys. Res. Lett.*, *27*, 3889–3892, 2000.

Wilson, R. J., and K. Hamilton, Comprehensive model simulation of thermal tides in the Martian atmosphere, *J. Atmos. Sci.*, *53*, 1290–1326, 1996.

Young, R. E., and G. Schubert, Dynamical aspects of the Venus 4-day circulation, *Planet. Space Sci.*, *21*, 1563–1580, 1973.

Zurek, R. W., Diurnal tide in the Martian atmosphere, *J. Atmos. Sci.*, *33*, 321–337, 1976.

Zurek, R. W., Atmospheric tidal forcing of the zonal-mean circulation: The Martian dusty atmosphere, *J. Atmos. Sci.*, *43*, 652–670, 1986.

Zurek, R. W., and R. M. Haberle, Zonally symmetric response to atmospheric tidal forcing in the dusty Martian atmosphere, *J. Atmos. Sci.*, *45*, 2469–2485, 1988.

Zurek, R. W., and L. J. Martin, Interannual variability of planet-encircling dust storms on Mars, *J. Geophys. Res.*, *98*, 3247–3259, 1993.

Zurek, R. W., J. R. Barnes, R. M. Haberle, J. B. Pollack, J. E. Tillman, and C. B. Leovy, Dynamics of the atmosphere of Mars, in *Mars*, edited by H. H. Kieffer et al., pp. 835–933, Univ. of Ariz. Press, Tucson, 1992.

S. R. Lewis and P. L. Read, Atmospheric, Oceanic and Planetary Physics, Clarendon Laboratory, Parks Road, Oxford OX1 3PU, England. (s.lewis1@physics.oxford.ac.uk; p.read1@physics.oxford.ac.uk)

Received May 2002; revised November 2002